Article

Mechanical Properties and Microstructure of W-6Ni-4Co Alloy by a Two-Step Sintering Process

Hongfeng Dong *, Peiyou Li, Taotao Ai and Wenhu Li

School of Materials Science and Engineering, Shaanxi University of Technology, Hanzhong 723001, China; lipeiyou112@163.com (P.L.); aitaotao0116@126.com (T.A.); ccwhli@163.com (W.L.)
* Correspondence: dhf@snut.edu.cn; Tel.: +86-0916-264-1622

Abstract: The mechanical properties and microstructure of W-6Ni-4Co alloy through solid phase sintering and two-step sintering process were investigated. The results demonstrated that the particle sizes of W-6Ni-4Co alloy milled powders increased firstly and decreased later during a mechanical alloying process. The shape of alloy milled powders affected that of grains in alloy by solid phase sintering. The shape of W-rich particles in the alloys changed from stripes to network, to polygonal and to subsphaeroidal finally during two-step sintering process. The mechanical properties could be attributed to the densification and microstructure of alloys, and increased during two-step sintering with short dwelling time.

1. Introduction

The W-based heavy alloys are two-phase composites consisting of body centered cubic (BCC) W phase with high density and face centered cubic (FCC) binder phase with good toughness and plasticity. The W-based alloys present superior properties including high strength, high radiation absorption and good corrosion resistance, proving suitable for many industrial applications including radiation shields, vibrating masses and counterweights [1–3]. In the W-based alloys, the W-Ni alloys are common engineering materials due to good intersolubility of Ni with W [4]. Adversely, a brittle Ni_4W phase can be easily generated because of uncontrollable solubility of W in Ni melts during liquid phase sintering, weakening the toughness of W-Ni alloys [5–7]. Therefore, some kinds of alloying element with good intersolubility and Ni are used in W-based multicomponent alloy, such as Cu, Co, Nb, Mo and Mn [8–12]. To control the recrystallization and grain growth of W-based multicomponent alloy during high temperature sintering, some kinds of nano-oxide particles such as La_2O_3, Y_2O_3, and HfO_2, have been added to the W-based alloys [13–15]. In our earlier work [16], the W-Ni-Cu alloy dispersed with Y_2O_3 particles has been investigated and suggested that the Y_2O_3 particles could restrain the dissolution and precipitation of W atoms in Ni-Cu liquid phase, as well as the growth of W crystals during sintering, strengthening mechanical properties of W-Ni-Cu alloy when the Y_2O_3 content was less than 0.4%. Recently, the development of W-Ni-Co alloy has been increasing attention due to the reinforcing effect of Co element on interfacial strength between tungsten and binder, enhancing both strength and ductility [9,17]. Chen et al. [18] studied the effect of Ni/Co ratios ranging from 2.3 to 9 on structure and properties of W-Ni-Co alloys. In their study, they found that a microstructure composed of the fine and uniformly distributed γ (Ni, Co) binder phase with a large amount of twinned structures was obtained, strengthening mechanical properties of W-Ni-Co alloys.

In the traditional production processes, cold pressing/sintering process is a popular method for W-based heavy alloys with large size and irregular shape. However, the cold pressing/sintering process is no constraint from die and needs to heat and cool for a long time during sintering, resulting in grain

growth even deformation [19,20]. Dinçer et al. [21] presented that W grains could exhibit physical collapse under gravity during liquid phase sintering, which leads to the agglomeration of W grains and exuding of the liquid phase due to the large density differences between W grains and the binder matrix phase. This problem could be overcome through the introduction of two-step sintering process. It is a double process with solid phase sintering and liquid phase sintering [22,23]. A skeleton structure can be formed through sintering neck of W grains by solid phase sintering, then densification will be completed quickly during liquid phase sintering, restraining grain growth of W phase.

In this paper, the effect of two-step sintering process on mechanical properties and microstructure of W-6Ni-4Co alloys were investigated. The present study aims to understand the densification, sintering behavior and strengthening process of the W-6Ni-4Co alloys in the two-step sintering procedures.

2. Experimental Procedure

W, Ni and Co powders (>99.7% purity) were used to prepare W-6Ni-4Co alloy. Their characteristics and mass fraction are presented in Table 1. W, Ni and Co powders were mass weighed, and the results are given in Table 1. The milling process was carried out by using a planetary ball mill (XQM-0.4A, Tenson Powder, Changsha, China) under an argon atmosphere for 25 h. An observational sampling was conducted every five hours. A tungsten carbide grinding medium with a ball to powder weight ratio of 3:1 was used. The milled powders were consolidated into green compacts with a pressure of 476 MPa, and then further two-step sintered in a high temperature tubular oven (GSL-1700X-II, Hefei ke jing materials technology CO., LTD, Hefei, China) under an argon atmosphere. The technology parameters are presented in Table 2. The two sintering curves are shown in Figure 1. The size of the sample after two-step sintering was 25 mm (length) × 6 mm (width) × 3 mm (height), and five samples under each sintering process were used for structure and property analysis. The samples for density testing were polished on six planes and wax-sealed to prevent the distilled water into pores of samples. The average size of ball milled powders was performed using a laser granularity analyzer (Rise-2008, Beijing shang de tong science and technology CO., LTD, Beijing, China). The phase composition of sintered samples was characterized using X-ray diffraction (D8 ADVANCE X, JEOL, Peabody, MA, USA) with Cu-Kα radiation, a step size of 0.05°, and a scan rate of 5°/min. Surface morphology was observed with scanning electron microscopy (SEM, JSM-6390LV, JEOL, Peabody, MA, USA) with energy dispersive spectrometer (EDS). The average grain sizes of sintered samples were also calculated using grid method. The densities of samples were evaluated using the Archimede's principle. Vickers hardness were performed at room temperature using a microhardness tester (HVS-1000, Shanghai Gaozhi Precision Instrument Co., LTD, Shanghai, China) and a load of 1 kg for 10 s, and the average microhardness at five vertical testing points is reported as the final result. The test samples for compressive strength measurements were obtained using a linear cutting machine. The total length of the test samples for the compressive strength measurements was Φ1.5 mm × 3 mm. The compressive strength and flexural strength of the sintered samples were tested using an MP-200 universal mechanical tester (Ji'nan Meitesi Testing Technology Co., LTD, Jinan, China) at a loading rate of 0.08 and 0.5 mm/min, respectively.
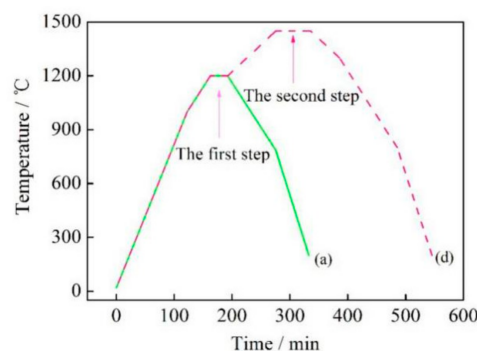

Figure 1. Sintering curves of **a** and **d**: (**a**) 1200 °C, 30 min; (**d**) 1450 °C, 60 min.

Table 1. Characteristics and mass fraction of W, Ni, and Co powders.

Element	Mass Fraction (wt. %)	Average Size (μm)	Preparation Method
W	90	3	Reduction
Ni	6	5	Electrolysis
Co	4	5	Electrolysis

Table 2. Technology parameters of two-step sintering.

Sintering Process	Process No. and Sample No.	Temperature /°C	Dwelling Time /min	Cooling Way
Solid phase sintering	a	1200	30	Furnace
Two-step sintering (a+)	b	1450	5	Furnace
	c	1450	20	Furnace
	d	1450	60	Furnace
	e	1500	5	Furnace
	f	1500	20	Furnace
	g	1500	60	Furnace

3. Results and Discussion

3.1. Characterization of W-6Ni-4Co Alloy Milled Powders

The SEM micrographs of W-6Ni-4Co alloy milled powders for 0, 5, 10, 15, 20 and 25 h are shown in Figure 2. The original shape of W powder is polyhedron, and those of Ni and Co are arborization, as shown in Figure 2a. After 5 h of milling, in Figure 2b, an increase of particle size was observed due to sheet and agglomeration of particles, indicating mass plastic deformation is the dominant milling processes, and the large surface area of powder enable the particles to weld together at this stage. With continued milling to 10 and 15 h, in Figure 2c,d, the sheet particle size increase because of cold welding. The average sizes of ball milled powders for 10 and 15 h are 6.4 and 7.5 μm, respectively. Until milling to 20 and 25 h, in Figure 2e,f, the particles become work hardened and fracture, leading to a reduction in particle size. The average sizes of ball milled powders for 20 and 25 h are 5.3 and 4.0 μm, respectivley. The results are the similar as that of Reference [18].
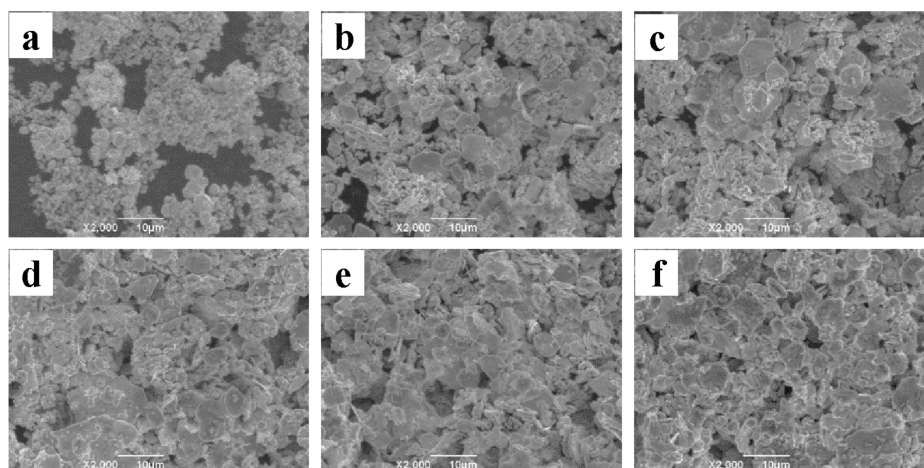

Figure 2. SEM images of W-6Ni-4Co alloy milled powders: (**a**) 0 h, (**b**) 5 h, (**c**) 10 h, (**d**) 15 h, (**e**) 20 h, (**f**) 25 h.

3.2. Relative Density of W-6Ni-4Co Alloys

Figure 3 is the effect of sintering process on the relative density of W-6Ni-4Co alloy. The W-6Ni-4Co alloy sintered by solid phase sintering at 1200 °C is slowly undergo densification, and its relative density is 78.7%. At 1450 °C for 5 min of two-step sintering, the relative density reaches 93.6%, revealing significant densification compared with that at 1200 °C of solid phase sintering. With the increase of dwelling time at 1450 °C, the relative density of the alloys shows a consistently increased trend, and it reaches 98% for 60 min. On the contrary, the relative density decrease with the increase of sintering temperature and dwelling time, and at 1500 °C for the final dwelling time of 60 min, the relative density of W-6Ni-4Co alloy is 97.5%.
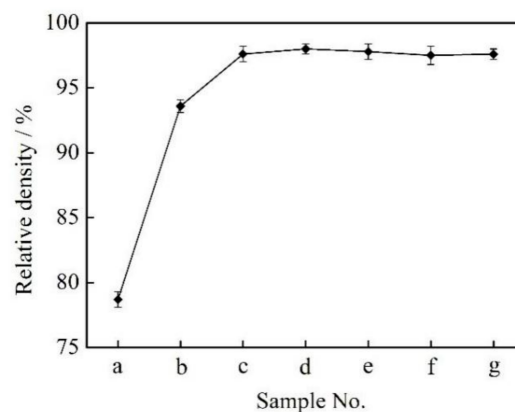

Figure 3. Relative density of W-6Ni-4Co alloys by the different sintering processes: (**a**) 1200 °C, 30 min; (**b**) 1450 °C, 5 min; (**c**) 1450 °C, 20 min; (**d**) 1450 °C, 60 min; (**e**) 1500 °C, 5 min; (**f**) 1500 °C, 20 min; (**g**) 1500 °C, 60 min.

From the change trend of relative density in W-6Ni-4Co alloys, the two-step sintering process could markedly enhance the densification of alloys and achieved nearly full densification of alloy at 1450 °C for 60 min due to volume shrinkage by strong diffusion of the binder phase into W-rich grains. By contrast, the alloys at 1500 °C exhibited the lower relative density, indicating the slower densification during liquid phase sintering. This is because a skeleton structure of W by solid phase sintering inhibit flow of liquid phase during liquid phase sintering, which makes volume shrinkage slower than that at 1450 °C for 60 min and decreases its density.

3.3. Microstructure Evolution of W-6Ni-4Co Alloy

Figure 4 presents the XRD patterns of the W-6Ni-4Co alloy by the different sintering processes. The volume fraction of phase was calculated by a formula as follows, and the results are shown in Table 3.

$$V_i = \frac{A_i}{\sum_{i=1}^{n} A_i} \times 100\%$$

where A_i presents the area of diffraction peaks of W, NiW and Co_3W phases, respectivley; V_i is the volume fractions of W, NiW and Co_3W phases, respectively.

The phases of W-6Ni-4Co alloy by the different sintering processes were composed of W, NiW and Co_3W phases. The volume fraction of NiW phase in the alloy at 1200 °C for 30 min is 4.58%, more than that of Co_3W phase due to its lower forming temperature of 1070 °C from binary phase diagram of Ni-W [24]. The relative volume fraction of NiW phase to Co_3W phase decreases during two-step sintering process. Moreover, it is obviously there is the most Co_3W phase than others, and it is 14.60% at 1500 °C for 5 min. This was because Co element can be melted at sintering temperature of 1500 °C, forming large amounts of Co liquid and dissolving W element rapidly, which caused great than or

equal to 3/1 of Co/W ratio, promoting the forming of Co$_3$W phase and adding volume fraction of Co$_3$W phase [25].
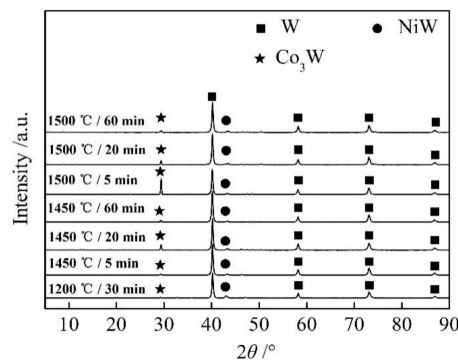

Figure 4. XRD patterns of the W-6Ni-4Co alloys by the different sintering processes.

Table 3. Volume fraction of W, NiW and Co$_3$W phases.

Sample No.	Volume Fraction of Phases/%		
	W	NiW	Co$_3$W
a	94.69	4.58	0.73
b	97.72	1.15	1.13
c	93.51	1.19	5.30
d	97.09	1.28	1.63
e	83.77	1.63	14.60
f	95.80	1.35	2.85
g	96.66	1.89	1.45

However, the Co$_3$W phase can be rarely formed when the Co liquid was not generating below a sintering temperature of 1495 °C or the W element was dissolved too much in Co liquid due to longer dwelling time of 20 and 60 min.

Figure 5 shows the SEM images of W-6Ni-4Co alloys, revealing their microstructure evolution during solid phase sintering and two-step sintering process. The average grain size of W-6Ni-4Co alloys was also calculated using grid method, as shown in Figure 5g. As shown in the Figure 5, the microstructure consists of white W-rich phase, gray binder phase and black pores. At a lower sintering temperature at 1200 °C, the W phase exhibits stripes and orientation arrangement perpendicular to cold pressing direction, and pores are unevenly distributed in the interface of W-binder phases, and the average grain size (2.3 μm) is smaller than others, indicating the obvious characteristic of solid phase sintering due to the lower sintering temperature below liquid phase sintering of 1453 °C. With the increase of sintering temperature to 1450 °C, the W-rich grains begin to grow and disperse into network, and the compact structure is also gradually formed, the similar as Figure 3. There were a lot of W-rich grains combing with one another to form a large W-rich grain with longer dwelling time. The average grain sizes at 1450 °C for 5, 20 and 60 min are 2.8, 2.9 and 3.5 μm, respectively.

The content of gray binder phase increased as the sintering temperature continues to increase to 1500 °C for 5 min (Figure 5e). The W-rich grains were polygonal and the average grain size was 3.3 μm at 1500 °C for 5 min. This is because that the liquid phase can be presented at 1500 °C, and a large number of Co$_3$W phases can form in the condition of instantaneous liquid phase sintering for 5 min. With the longer dwelling time, the W-rich grains growth reach 3.9 μm, in Figure 3f, and the content of gray binder phase decreased due to inhibition of Co$_3$W phase forming by sufficiently diffusion of W in Co during liquid phase sintering. At 1500 °C for 60 min, the W-rich grains continued to grow into subsphaeroidal, and the average grain size is 3.9 μm (Figure 5g). It can be seen the average grain size of alloys by two-step sintering at the temperature of 1500 °C is obviously smaller than that of

Reference [21] by liquid phase sintering at 1500 °C. This is because dissolution and precipitation in liquid phase and physical collapse of W during liquid phase sintering would be prevented by skeleton structure resulting from the first step of solid phase sintering. To verify the distribution of W-rich and binder phases, the EDS analysis have been conducted as alloy at 1450 °C for 60 min for an example, as shown in Figure 6.
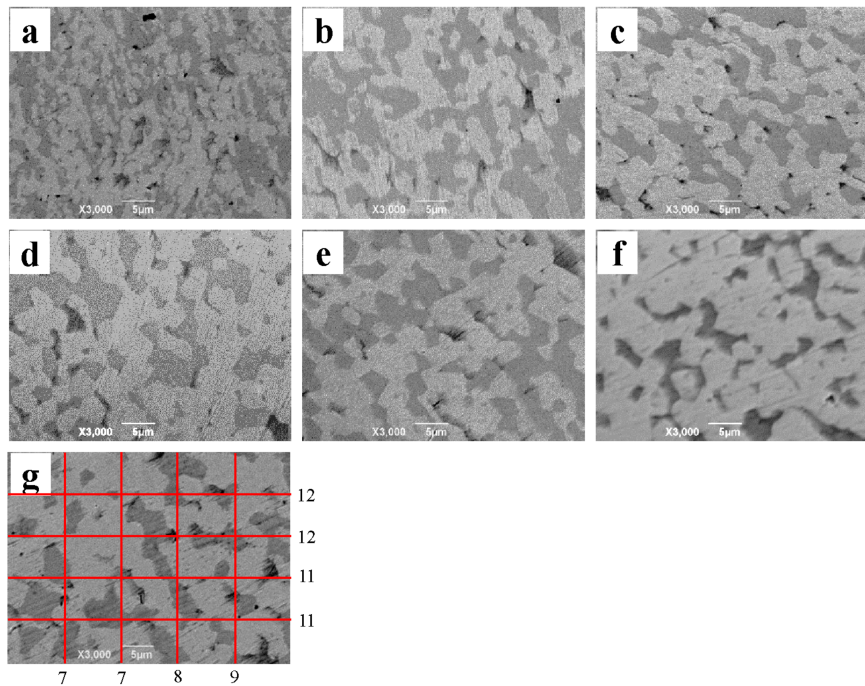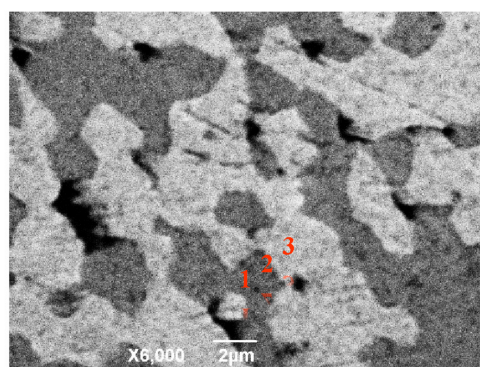

Figure 5. SEM images of W-6Ni-4Co alloys by the different sintering processes: (**a**) 1200 °C, 30 min; (**b**) 1450 °C 5 min; (**c**)1450 °C, 20 min; (**d**) 1450 °C, 60 min; (**e**) 1500 °C, 5 min; (**f**) 1500 °C, 20 min; (**g**) 1500 °C, 60 min.

Position	Composition / wt. %		
	W	Ni	Co
1	71.387	16.091	12.522
2	88.978	6.443	4.579
3	98.454	0.837	0.709

Figure 6. EDS analysis of alloy at 1450 °C for 60 min.

As a consequence, the W-rich grains kept stripes the similar as W-6Ni-4Co alloy milled powders, and is difficult to grow at 1200 °C for 30 min. Moreover, the process of densification is also restrained due to the lower temperature during solid phase sintering. At 1450 °C, the interdiffusion of Co, Ni and W elements during solid phase sintering is more active, and the phases are uniform distribution, and begin to grow. Despite that, this alloy is markedly finer than traditional W alloys, and was typical fine-grained W alloy materials. This finding indicated that the two-step sintering process could effectively control grain growth for W alloys by skeleton structure through sintering neck of W grains during the first solid phase sintering and later rapid alloying. At 1500 °C for 5 min, the grains did not grow significantly during liquid phase sintering due to the weaker dissolution and precipitation

effect of instantaneous liquid phase sintering. When the dwelling time was further prolonged from 5 to 60 min, resulting in the further growth of grains. The W-rich grains changed from polygonal to subsphaeroidal due to the stronger dissolution and precipitation effect of long time liquid phase sintering. To improve the density and restrain the grain growth of W alloys, the best method is to increase the sintering temperature suitably, rather than to prolong the dwelling time.

3.4. Mechanical Properties of W-6Ni-4Co Alloy

Figure 7 shows the microhardness (HV), flexural strength (σ_{bb}) and compressive strength (σ_b) of W-6Ni-4Co alloys by different sintering process, and the data are listed in Table 4. The offset 0.2% yield strength ($\sigma_{0.2}$) and compressive toughness (A_t) were calculated though the true stress–strain curves for compressive testing, as shown in Figure 8. At the sintering temperature of 1200 °C, the microhardness of the alloy is the lowest at 258.63 HV. During the increase in sintering temperature to 1450 °C, the microhardness of the alloy showed the highest at 596.47 HV, more than that of alloys by one-step sintering at 1450 °C in references [9] and [18] because of refine grain strengthening and network strengthening effect of W. This could be attributed to the synergistic effect of densification and network distribution of W-rich phase [18], which is optimized during two-step sintering process at 1450 °C for 5 min. However, the microhardness of the alloy begins to decrease with the longer dwelling time from 5 to 60 min. This is because the W-rich grains are combined with one another to form a large W-rich grain, and the distribution of gray binder phase exhibits nonuniform, as shown in Figure 5b–d. At 1500 °C for 5 min, the microhardness of the alloy is 559.13, less than that of alloys at 1450 °C for 5 and 20 min for its rapid grain growth during liquid phase sintering. With the longer dwelling time at 1500 °C, the microhardness decreased firstly and then increased due to grain growth. The compressive strength of W-6Ni-4Co alloys presented similar change trend as the microhardness, which could be also attributed to the synergistic effect of densification, grain refining and distribution of the binder phase [18]. The compressive strength of alloys at 1500 °C for 5 min exhibits the highest at 2483.50 MPa because of Co_3W phase with close-packed phase $L1_2$ structure during instantaneous liquid phase sintering, resulting in a strong interface phase strengthening effect. Moreover, the yield strength and compressive toughness have the similar change trend as compressive strength, and the alloys shows the highest yield strength of 1437.40 MPa at 1450 °C for 5 min, and the highest compressive toughness of 624.72 J·cm^{-3} at 1500 °C for 5 min. Different from the variation trends of microhardness and compressive strength, the flexural strength of alloys increased with increase of sintering temperature and dwelling time under 1450 °C for 60 min, and then decreased firstly and increased later with increase of dwelling time at 1500 °C. The alloys at 1500 °C for 20 min displayed the highest flexural strength at 1849.70 MPa.
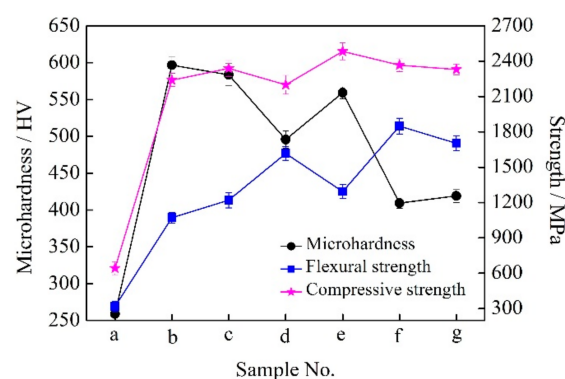

Figure 7. Microhardness, flexural strength and compressive strength of W-6Ni-4Co alloys by the different sintering processes: (**a**) 1200 °C, 30 min; (**b**) 1450 °C, 5 min; (**c**) 1450 °C, 20 min; (**d**) 1450 °C, 60 min; (**e**) 1500 °C, 5 min; (**f**) 1500 °C, 20 min; (**g**) 1500 °C, 60 min.
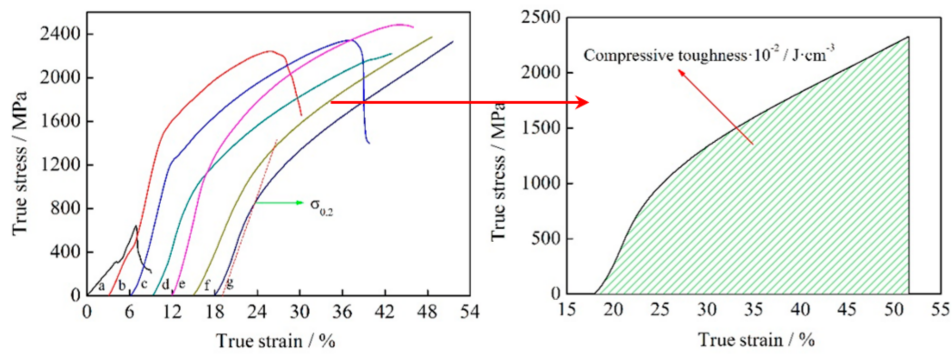
Figure 8. True stress–strain curves for compressive testing and schematic diagram of yield strength and compressive toughness for W-6Ni-4Co alloys by the different sintering processes: (**a**) 1200 °C, 30 min; (**b**) 1450 °C, 5 min; (**c**) 1450 °C, 20 min; (**d**) 1450 °C, 60 min; (**e**) 1500 °C, 5 min; (**f**) 1500 °C, 20 min; (**g**) 1500 °C, 60 min.

Table 4. Results of mechanical properties of W-6Ni-4Co alloy by the different sintering processes, such as microhardness (HV), flexural strength (σ_{bb}), compressive strength (σ_b), yield strength ($\sigma_{0.2}$) and compressive toughness (A_t).

Sample No.	HV	σ_{bb}/MPa	σ_b/MPa	$\sigma_{0.2}$/MPa	A_t/J·cm^{-3}
a	258.63	318.60	642.80	307.73	25.69
b	596.47	1072.20	2240.20	1437.40	434.90
c	583.60	1220.40	2338.40	1211.82	568.59
d	495.53	1616.70	2200.70	779.56	509.97
e	559.13	1293.70	2483.50	1104.58	624.72
f	409.23	1849.70	2366.70	944.66	509.73
g	419.20	1703.00	2330.10	687.85	494.51

Obviously, the mechanical properties of W-6Ni-4Co alloys by different sintering process have a close relationship with the average grain size of alloys. To understand the relationship between mechanical properties, and average grain size of alloys more directly, the change curves of yield strength and average grain size of alloys are shown in Figure 9, presenting the opposite trend of mechanical properties and average grain size.
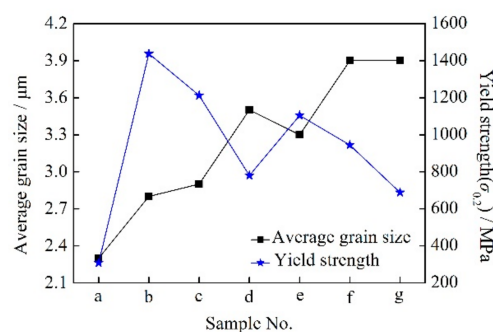

Figure 9. Relation of yield strength and average grain sizes of W-6Ni-4Co alloys by the different sintering processes: (**a**) 1200 °C, 30 min; (**b**) 1450 °C, 5 min; (**c**) 1450 °C, 20 min; (**d**) 1450 °C, 60 min; (**e**) 1500 °C, 5 min; (**f**) 1500 °C, 20 min; (**g**) 1500 °C, 60 min.

As shown in the true stress–strain curves for compressive testing of W-6Ni-4Co alloys by different sintering process, see Figure 9, the slope of curves at elastic deformation area of samples by two-step sintering were higher than that by solid phase sintering process, indicating better stiffness. The plastic strain of alloy at 1200 °C for 30 min is about 5%, and much smaller than that (≥24%) by

two-step sintering. The plastic strain of alloy at 1500 °C for 5 min is the highest (≈30%), indicating the best ductility.

Figure 10 shows the true stress–strain curves for flexural testing of W-6Ni-4Co alloys by different sintering process. As shown in Figure 10, the alloys sintering from 1200 °C for 30 min to 1500 °C for 5 min show the brittle behavior, while some plastic deformation is exhibited at 1500 °C for 20 and 60 min, therefore, the brittle-to-ductile transition displayed between 5 and 20 min at 1500 °C. Thus, the W-6Ni-4Co alloys are characterized by excellent comprehensive property during two-step sintering with short dwelling time of 5 min at 1450 and 1500 °C. As dwelling time increases from 5 min to 60 min, the samples underwent sufficient alloying and strong dissolution, and precipitation effect of W in binder phase, promoting grain growth, which can weaken properties of W-6Ni-4Co alloys.
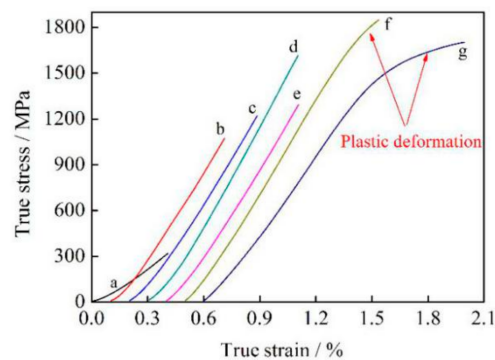

Figure 10. True stress–strain curves for flexural testing of W-6Ni-4Co alloys by the different sintering processes: (**a**) 1200 °C, 30 min; (**b**) 1450 °C, 5 min; (**c**) 1450 °C, 20 min; (**d**) 1450 °C, 60 min; (**e**) 1500 °C, 5 min; (**f**) 1500 °C, 20 min; (**g**) 1500 °C, 60 min.

3.5. Fracture Morphology of W-6Ni-4Co Alloy

The variation trend of the mechanical properties of the samples are closely related to the microstructural characteristics. Figure 11 shows the fracture morphology for flexural testing of W-6Ni-4Co alloy. There is four fracture modes, namely W cleavage (I), binder phase rupture (II), W–W grain boundary separation (III), and W-binder phase interface separation (IV). For the 1200 °C sintering samples, the densification of the sample is the lowest, reaching 78.7%, and the porosity of the alloy is more (Figure 5a). At this temperature, the fracture modes mainly involve W–W grain boundary separation (III); thus, the flexural strength is the lowest (Table 4). When the sample is sintered at 1450 °C, the densification degree of the alloy observably increases, and the fracture mode mainly occur in the W cleavage (I), binder phase rupture (II), W–W grain boundary separation (III), and W-binder phase interface separation (IV). Moreover, with the longer dwelling time from 5 to 60 min, the percentage of W cleavage (I) and binder phase rupture (II) increase, indicating strong interface bonding for network structure of W-rich phase with longer alloying process (Figure 5), and promoting flexural strength, as shown in Figure 7. The percentage of W–W grain boundary separation (III) is the most in sample at 1500 °C for 5 min due to weaker interface bonding during instantaneous liquid phase sintering. When the dwelling time prolonged to 20 min at 1500 °C, the W cleavage (I) and binder phase rupture (II) are the main fracture modes. This is caused by strong interface bonding because of long liquid phase sintering, resulting in the strongest flexural strength of the alloy. As the dwelling time continues to 60 min at 1500 °C, the W–W grain boundary separation (III) and W-binder phase interface separation (IV) are main fracture modes. This is because the network W-rich phase would be broken partly by liquid phase flow for a long time, weakening network strengthening effect, which make the flexural strength of the alloy decrease in Figure 7.
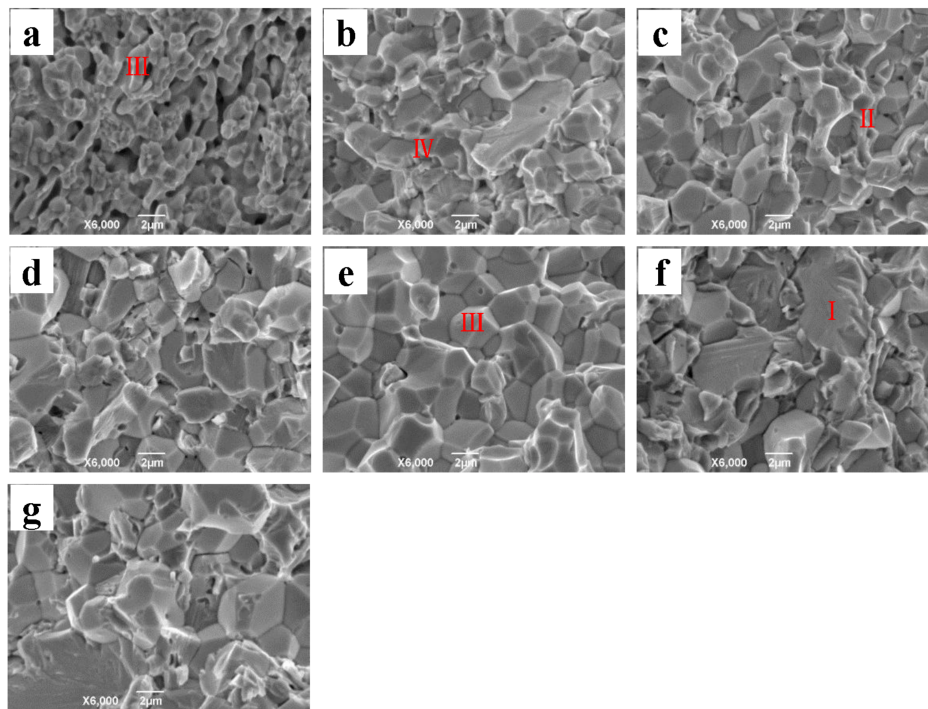
Figure 11. Fracture morphology for flexural testing of W-6Ni-4Co alloys by the different sintering processes: (**a**) 1200 °C, 30 min; (**b**) 1450 °C, 5 min; (**c**) 1450 °C, 20 min; (**d**) 1450 °C, 60 min; (**e**) 1500 °C, 5 min; (**f**) 1500 °C, 20 min; (**g**) 1500 °C, 60 min.

4. Conclusions

The W-6Ni-4Co alloy was prepared by solid phase sintering and two-step sintering processes. The corresponding characterization of alloy milled powders and alloy sintered were analyzed and the results demonstrated that:

(1) The particle size of W-6Ni-4Co alloy milled powders increased firstly due to sheet and agglomeration of particles and decreased later for fracture of particles during a mechanical alloying process.

(2) The shapes of W-rich particles changed from stripes to network, to polygonal and to subsphaeroidal finally, and the best compact structure formed at sintering temperature of 1450 °C and dwelling time of 60 min.

(3) The samples were characterized by excellent comprehensive property during two-step sintering with short dwelling time of 5 min. The best results of microhardness, compressive strength, flexural strength, yield strength and compressive toughness are 596.5 HV, 2483 MPa and 1850 MPa, 1437 MPa and 625 J·cm^{-3} respectively. The mechanical properties can be attributed to the synergistic effect of densification, grain refining and distribution of the W-rich phase and binder phase.

References

1. Sengupta, P.; Debata, M. Effect of partial and full substitution of Ni with NiB on densification, structure and properties of 90W-6Ni-2Fe-2Co heavy alloys. *J. Alloys Compd.* **2019**, *774*, 145–152. [CrossRef]
2. Zhuo, L.; Zhang, Y.; Zhao, Z.; Luo, B.; Chen, Q.; Liang, S. Preparation and properties of ultrafine-grained W-Cu composites reinforced with tungsten fibers. *Mater. Lett.* **2019**, *243*, 26–29. [CrossRef]
3. Hu, K.; Wang, G.H.; Li, X.Q.; Qu, S.G. Microstructure and formation mechanism in a surface carburized tungsten heavy alloy. *J. Alloys Compd.* **2019**, *787*, 560–569. [CrossRef]
4. Gu, D.; Li, Y.; Wang, H.; Jia, Q.; Zhang, G. Microstructural development and its mechanism of mechanical alloyed nanocrystalline W-10Ni alloy reinforced with Y_2O_3 nanoparticles. *Int. J. Refract. Met. Hard Mater.* **2014**, *44*, 113–122. [CrossRef]
5. Ding, L.; Xiang, D.; Pan, Y.; Li, Y. Mechanical properties and microstructural evolution of Mo-Co-co-strengthened W-Ni-Fe alloys by spark plasma sintering. *J. Alloys Compd.* **2017**, *712*, 593–598. [CrossRef]
6. Patra, A.; Meraj, M.; Pal, S.; Yedla, N.; Karak, S.K. Experimental and atomistic simulation based study of W based alloys synthesized by mechanical alloying. *Int. J. Refract. Met. Hard Mater.* **2014**, *58*, 57–67. [CrossRef]
7. Patra, A.; Sahoo, R.R.; Karak, S.K.; Sahoo, S.K. Effect of nano Y_2O_3 dispersion on thermal, microstructure, mechanical and high temperature oxidation behavior of mechanically alloyed W-Ni-Mo-Ti. *Int. J. Refract. Met. Hard Mater.* **2018**, *70*, 134–154. [CrossRef]
8. Kilic, M.; Ozyurek, D.; Tuncay, T. Dry Sliding wear behavior and microstructure of the W-Ni-Fe and W-Ni-Cu heavy alloys produced by powder metallurgy technique. *Powder. Metall. Met. C* **2016**, *55*, 73–84. [CrossRef]
9. Chen, C.; Ma, S.H. Study on characteristics and sintering behavior of W-Ni-Co tungsten heavy alloy by a secondary ball milling method. *J. Alloys Compd.* **2018**, *731*, 78–83. [CrossRef]
10. Saxena, R.; Patra, A.; Karak, S.K.; Ciupinski, L. Fabrication and characterization of nano-Y_2O_3 dispersed W-Ni-Nb alloys. *Int. J. Refract. Met. Hard Mater.* **2018**, *71*, 70–78. [CrossRef]
11. Patra, A.; Saxena, R.; Karak, S.K.; Laha, T.; Sahoo, S.K. Fabrication and characterization of nano-Y_2O_3 dispersed W-Ni-Mo and W-Ni-Ti-Nb alloys by mechanical alloying and spark plasma sintering. *J. Alloys Compd.* **2017**, *707*, 245–250. [CrossRef]
12. Pan, Y.; Ding, L.; Xiang, D. Microstructure evolution and mechanical properties of spark plasma sintered W-Ni-Mn alloy. *Trans. Nonferrous Met. Soc. Chin.* **2017**, *27*, 1588–1593. [CrossRef]
13. Chen, Y.; Wu, Y.; Yu, F.; Chen, J. Microstructure and mechanical properties of tungsten composites co-strengthened by dispersed TiC and La_2O_3 particles. *Int. J. Refract. Met. Hard Mater.* **2008**, *26*, 525–529. [CrossRef]
14. Kim, Y.; Lee, S.; Kim, E.P.; Noh, J.W. Effects of ThO_2 on the solid) state sintering behavior of W-Ni-Fe alloy. *Int. J. Refract. Met. Hard Mater.* **2011**, *29*, 112–116. [CrossRef]
15. Cui, K.; Shen, Y.; Yu, J.; Ji, B. Microstructural characteristics of commercial purity W and W-1% La_2O_3 alloy. *Int. J. Refract. Met. Hard Mater.* **2013**, *41*, 143–151. [CrossRef]
16. Li, W.; Dong, H. Effect of nano-Y_2O_3 on microstructure and mechanical properties of W-Ni-Cu alloys. *Mater. Res. Express* **2018**, *5*, 106503. [CrossRef]
17. Chen, C.; Ma, S.H. Study on combination of in-situ dispersion and secondary ball milling for W-Ni-Co tungsten heavy alloy. *Int. J. Refract. Met. Hard Mater.* **2018**, *71*, 8–14. [CrossRef]
18. Chen, C.; Ma, S.H. Effects of Ni/Co ratio and mechanical alloying on characteristics and sintering behavior of W-Ni-Co tungsten heavy alloys. *J. Alloys Compd.* **2017**, *711*, 488–494. [CrossRef]
19. Hamidi, A.G.; Arabi, H.; Khaki, J.V. Sintering of a nano-crystalline tungsten heavy alloy powder. *Int. J. Refract. Met. Hard Mater.* **2019**, *80*, 204–209. [CrossRef]
20. Shi, K.; Huang, B.; He, B.; Xiao, Y.; Yang, X.; Lian, Y.; Liu, X.; Tang, J. Room-temperature tensile strength and thermal shock behavior of spark plasma sintered W-K-TiC alloys. *Nucl. Eng. Technol.* **2019**, *51*, 190–197. [CrossRef]
21. Dinçer, O.; Pehlivanoğlu, M.K.; Çalişkan, N.K.; Karakaya, İ.; Kalkanli, A. Processing and microstructural characterization of liquid phase sintered tungsten–nickel–cobalt heavy alloys. *Int. J. Refract. Met. Hard Mater.* **2015**, *50*, 106–112. [CrossRef]
22. Jung, W.K.; Ma, H.J.; Kim, D.G.; Kim, D.K. Two-step sintering behavior of titanium-doped Y_2O_3 ceramics with monodispersed sub) micrometer powder. *Ceram. Int.* **2019**, *45*, 510–515. [CrossRef]

23. Fan, Z.S.; Xiang, D.P.; Pan, Y.L.; Jiang, H. Effect of two-time spark plasma sintering on microstructure and mechanical properties of W-6Ni-4Mn alloy. *Mater. Sci. Eng. A* **2019**, *745*, 300–306. [CrossRef]

24. Sato, J.; Omori, T.; Oikawa, K.; Ohnuma, I.; Kainuma, R.; Ishida, K. Co-based high-temperature alloys. *Science* **2006**, *312*, 90–91. [CrossRef] [PubMed]

25. Nagasaki, S.; Hirabayashi, M. *Binary Alloy Phase-Diagrams*; AGNE Gijutsu Center, Co., Ltd.: Tokyo, Japan, 2002.